Entropy Production by Underdamped Langevin Dynamics

Jinghao Lyu,[*] Kyle J. Ray,[†] and James P. Crutchfield[‡]

Complexity Sciences Center and Physics and Astronomy Department,
University of California at Davis, One Shields Avenue, Davis, CA 95616

(Dated: May 21, 2024)

Entropy production (EP) is a central quantity in nonequilibrium physics as it monitors energy dissipation, reversibility, and free energy differences during thermodynamic transformations. Estimating EP, however, is challenging both theoretically and experimentally due to limited access to the system dynamics. For overdamped Langevin dynamics and Markov jump processes it was recently proposed that, from thermodynamic uncertainty relations (TUR), short-time cumulant currents can be used to estimate EP without knowledge of the dynamics. Yet, estimation of EP in underdamped Langevin systems remains an active challenge. To address this, we derive a modified TUR that relates the statistics of two specific novel currents—one cumulant current and one stochastic current—to a system's EP. These two distinct but related currents are used to constrain EP in the modified TUR. One highlight is that there always exists a family of currents such that the uncertainty relations saturate, even for long-time averages and in nonsteady-state scenarios. Another is that our method only requires limited knowledge of the dynamics—specifically, the damping-coefficient to mass ratio and the diffusion constant. This uncertainty relation allows estimating EP for both overdamped and underdamped Langevin dynamics. We validate the method numerically, through applications to several underdamped systems, to underscore the flexibility in obtaining EP in nonequilibrium Langevin systems.

Keywords: nonequilibrium thermodynamics, thermodynamic uncertainty relations, dissipation

I. INTRODUCTION

Over the past decade stochastic thermodynamics led to significant advances in our understanding of nonequilibrium systems. One highlight is the *thermodynamic uncertainty relation* (TUR) that gives the trade-off between *entropy production* (EP) Σ (or *dissipation*) and the resolution (or *accuracy*) of a current J:

$$\text{var}(J) \cdot \frac{\Sigma}{2} \geq \langle J \rangle^2 \ , \tag{1}$$

where $\text{var}(J)$ and $\langle J \rangle$ are the variance and mean of J, respectively. After its first discovery in the nonequilibrium steady state (NESS) regime [1–4], the TUR was extended to non-NESS discrete Markovian systems [5], overdamped Langevin systems [6], underdamped Langevin systems [7], active particles [8], processes with measurement and feedback control [9], and more [10–27]. Generally speaking, TURs, provide lower bounds on the EP using observable currents. An array of techniques are used to derive these TURs, including large deviation theory [2], the Crámer-Rao bound [28], the characteristic function inequality [6, 29], and the Cauchy-Schwartz inequality [30].

EP is a key physical property of a thermodynamic transformation—often taken as a proxy for energy dissipation. It describes how irreversible a transformation is and quantifies the minimal thermodynamic resources to drive it. Saturating a TUR inequality allows estimating the EP (rate) directly from observed data. This reduces to an optimization problem: find a current J that maximizes $2\langle J \rangle^2 / \text{var}(J)$. That maximum is the EP. Recently, in the short-time duration limit, it was proposed that equality holds for several specific currents [31–35]. Using this, EP can be estimated without detailed knowledge of the forces in overdamped Langevin systems or the transition rates in Markovian systems. A natural follow-on then is: Can we use currents to estimate EP in other stochastic systems? Here, we focus on solving this problem for underdamped Langevin dynamics.

Several modified TURs for underdamped systems exist already [7, 36–39], but none are well suited for empirically estimating EP. The main difference in the underdamped case, compared to overdamped, is the appearance of reversible currents in the dynamics. And, these result in modified TURs with additional terms; for example, the total activity or the Fisher information. Some TURs also require settings with perfect control and knowledge of all protocol parameters. Such requirements are typically impossible to meet in experiments. Furthermore, the physical meaning and tightness of these modified TURs for underdamped systems are not clear, even in the short-time regime.

The following directly addresses EP estimation in the underdamped regime. We introduce two different types of current—irreversible currents and stochastic currents—and derive a TUR that relates their moments to EP. We show that this TUR (i) applies to all Langevin (overdamped and underdamped) systems, (ii) works under arbitrary control protocols, (iii) is always saturable, and (iv) is not limited to short time or NESS inference. This TUR can be used to readily estimate EP

---

[*] jolyu@ucdavis.edu
[†] kjray@ucdavis.edu
[‡] chaos@ucdavis.edu

from experimental measurements provided only that the system's damping-coefficient to mass ratio and the diffusion constant are known.

II. DYNAMICS

We consider a n-dimensional underdamped motion at the temperature T. The Langevin equations are:

$$dx = \frac{p}{m}dt \ , \ dp = -\gamma\frac{p}{m}dt + F(x,t)dt + dB_t \ , \quad (2)$$

where x, p, F, γ, and m are the position, momentum, external force, damping coefficient, and particle mass, respectively. dB_t are n-dimension independent infinitesimal Brownian motions—Wiener processes with variance $2Ddt$ where $D = \gamma k_B T$ is the duffision constant. Throughout, we assume the Boltzmann constant $k_B = 1$.

The corresponding evolution of the probability distribution $f(x, p, t)$ from $t = 0$ to τ is described by a continuity constraint called Kramer's equation:

$$\partial_t f(x, p, t) = -\left(\frac{p}{m} \cdot \partial_x f(x, p, t) + \partial_p\left(u_p f(x, p, t)\right)\right) , \quad (3)$$

where $u_p = -\gamma\frac{p}{m} + F(x, t) - \gamma T \partial_p \log f(x, p, t)$ is the probability velocity along p. We decompose u_p into u_p^{rev} and u_p^{irr} based on how they behave under the time reverse transformation $x \to x, p \to -p$: $u_p^{\text{rev}} \to u_p^{\text{rev}}$ and $u_p^{\text{irr}} \to -u_p^{\text{irr}}$. The following assumes $u_p^{\text{rev}} = F(x, t)$ and $u_p^{\text{irr}} = -\gamma\frac{p}{m} - \gamma T \partial_p \log f(x, p, t)$.

We take the average EP of such a system to be the sum of the mean heat flux into the thermal environment and the change in Shannon entropy over the system's probability distribution function. The average EP can be written as:

$$\Sigma = \frac{1}{\gamma T} \int_0^\tau dt \int dx dp \ u_p^{\text{irr}}(x, p, t)^2 f(x, p, t) . \quad (4)$$

(See Appendix A for details.) As we can see, the total EP is the sum of the sub-EP in each direction and generalizations to higher dimensions are straightforward given a method for estimating Σ along any given direction. For clarity, we discuss only the sub-EP from here on out and assume a one-dimensional system.

III. CURRENTS AND MODIFIED TURS

While our primary focus is a method for estimating EP in underdamped systems, the underlying method applies to overdamped systems as well. We first consider currents and TURs in overdamped dynamics and then extend the method to underdamped systems.

A. Overdamped dynamics

Analogous to Eq. (4), in a one-dimensional overdamped system described by a probability distribution $f(x, t)$, the mean EP can be expressed as:

$$\Sigma = \frac{1}{D} \int_0^\tau dt \int dx f(x, t) u^2(x, t) . \quad (5)$$

where $u(x, t)$ is the probability current velocity. A *cumulant current* $J(w)$ is the integral of a local weight function $w = w(x, t)$ over a particular trajectory Γ:

$$J(w) = \int_\Gamma w(x, t) \circ dx \ , \quad (6)$$

where the $\circ$ represents a Stratonovich product. The average of this current over all trajectories is [40]:

$$\langle J(w) \rangle = \int_0^\tau dt \int dx f(x, t) u(x, t) w(x, t) . \quad (7)$$

From this point forward, $\langle \cdots \rangle$ denotes averaging a trajectorywise quantity over all possible trajectories.

Inspired by Ref. [30], we define a conjugate *stochastic current* J_S with the same weight $w(x, t)$ as the physical current J:

$$J_S(w) = \int_\Gamma w(x, t) \cdot dB_t \ , \quad (8)$$

where $\cdot$ denotes an Ito product. The stochastic current's statistical moments are imbued with special properties. First, J_S has zero mean and so $\langle J_S^2 \rangle = \text{var}(J_S)$. Second, the covariance of the product of two stochastic currents is related to a particular cumulant current:

$$\langle J_S(w) J_S(w') \rangle = \left\langle \int_{\Gamma \times \Gamma} dB_{t_1} dB_{t_2} w(x_{t_1}, t_1) w'(x_{t_2}, t_2) \right\rangle$$
$$= 2D \int_0^\tau dt \int dx \ f(x, t) w(x, t) w'(x, t)$$
$$= 2D \langle J(ww'/u) \rangle . \quad (9)$$

The relation above motivates a specific stochastic current, also defined in Ref. [30]:

$$A_t \equiv \frac{1}{2D} J_S(u) \ ,$$

which can be seen to satisfy both $\langle A_t^2 \rangle = \langle J(u) \rangle = \Sigma/2$ and $\langle A_t J_S(w) \rangle = \langle J(w) \rangle$ using the property above.

Now, suppressing the dependence on the specific w and applying the Cauchy-Schwartz inequality, yields:

$$\langle A_t^2 \rangle \langle J_S^2 \rangle \geq \langle A_t J_S \rangle^2 . \quad (10)$$

Plugging in the relations for A_t gives a TUR valid for any choice of $w(x, t)$:

$$\frac{\Sigma}{2} \geq \frac{\langle J \rangle^2}{\text{var}(J_S)} \ . \quad (11)$$

This inequality can be saturated if and only if $w(x,t) = cu(x,t)$, where c is a constant. Also, note that there are two different types of current in our uncertainty relation. While J_S is not a physically observable current, its variance can be readily calculated by using Eq. (9):

$$\text{var}(J_S(w)) = 2D\langle J(w^2/u)\rangle$$
$$= 2D\left\langle \int_\Gamma w(x,t)^2 dt \right\rangle . \tag{12}$$

This form shows that the quantity is as readily estimated from experimental trajectories as the cumulant current average. It also shows clearly that $\text{var}(J_S)$ converges to $\text{var}(J)$ as $\tau \to 0$, reducing Eq. (11) to previous results on short-time duration inference [31–35].

B. Underdamped

The same approach yields a TUR for the underdamped regime. Naively, we simply promote our trajectories, integrals, and weight functions to be defined over the (x, p) phase space: $w = w(x, p, t)$ and cumulant currents $\int w(x, p, t) \circ dp$. We maintain the same definition of $J_S = \int_\Gamma w(x, p, t) \cdot dB_t$ and, by looking at Eq. (4), we define $A = J_s(u_p^{\text{irr}})/2D$ to recover $\langle A^2 \rangle = \Sigma/2$.

Continuing as before, we investigate the average of the product of A and J_S, finding that $\langle AJ_S(w)\rangle = \langle wu_p^{\text{irr}}\rangle$. However, this is not the average of the naively promoted cumulant current $\int w(x, p, t) \circ dp$. Thus, to display the necessary average behavior, we require a current such that $\langle J(w)\rangle = \langle wu_p^{\text{irr}}\rangle$—one that only accounts for the irreversible part of the probability current, rather than the full probability current. The naive extension of our overdamped current fails, but the following definition suffices:

$$J(w) = \int_\Gamma w(x, p, t)\gamma dx - \frac{1}{2}\int_\Gamma dw \cdot dp \tag{13}$$

(See App. B for more details). Again, using the Cauchy-Schwartz inequality:

$$\langle A^2\rangle\langle J_S^2\rangle \geq \langle AJ_S\rangle^2 . \tag{14}$$

We recover Eq. (11) where the equality holds if and only if $w(x, p, t) \sim u_p^{\text{irr}}(x, p, t)$. Notably, this TUR holds for completely arbitrary over- or underdamped Langevin dynamics (over any timescale for any time-dependent driving force and any initial probability). It is not limited by being valid only for certain regimes, initial conditions, timescales, or driving forces.

IV. ESTIMATING EP

In experiments, we observe discretized trajectories of Langevin dynamics: $\Gamma_{\text{dis}} = \{(x_i, p_i/m, t_i)\}_{i=0}^N$, where x_i and p_i are the position and momentum at time $t_i = i \cdot$

τ/N. Suppose we observe N_Γ trajectories and pick a weight function $w(x, p, t)$. The average $\langle J\rangle$ and $\text{var}(J_S)$ can be estimated by averaging J_Γ of each trajectory. In underdamped systems:

$$\langle J\rangle = \tag{15}$$
$$\left\langle \sum_{i=0}^{N-1} \left(\gamma w_i(x_{i+1} - x_i) - \frac{1}{2}(w_{i+1} - w_i)(p_{i+1} - p_i)\right) \right\rangle$$

$$\text{var}(J_S) = 2D\left\langle \sum_{i=0}^{N-1} w_i^2 dt \right\rangle , \tag{16}$$

where w_i is the weight function evaluated at (x_i, p_i, t_i).

In this way, estimating EP becomes an optimization problem:

$$\widehat{\Sigma} = \max_w \frac{2\langle J\rangle^2}{\text{var}(J_S)} . \tag{17}$$

Compared to the method used in Refs. [33–35, 41], our bound is always saturable for any time dependent drive over any time scale. However, we also need additional knowledge: the damping coefficient, the mass and the diffusion constant. Since we can rescale $w(x, p, t)$ freely, only the damping-coefficient to mass ratio γ/m and diffusion constant are needed.

Finding the optimal expression of $w(x, p, t)$ for an arbitrarily time-varying system is challenging in general. A good model class for such a weight w could contain millions of parameters. To demonstrate our results, though, we follow Ref. [34] and use a set of Gaussian basis functions $\{\phi_i\}_i$ to approximate the weight.

There are two ways to expand general time-dependent weights $w(x, p, t)$. We can let either coefficients or basis functions have time dependence:

$$w(x, p, t) \sim \sum_i \begin{cases} c_i \cdot \phi_i(x, p, t) & (t \text{ in basis functions}) \\ c_i(t) \cdot \phi_i(x, p) & (t \text{ in coefficients}) \end{cases} . \tag{18}$$

We refer to estimations based on these two expansions as *rate-based estimations* and *one-shot estimations*, respectively. The meaning of these names will become clear.

By picking basis functions to approximate the weight, the optimal weight w_{opt} for a given sample of trajectories can be written in a closed form. To avoid overfitting to small data sets, we also include L-2 norm regularization. (Details for the exact regularized solution can be found in Appendix C.) In all cases, we use equal-width multivariate Gaussian basis functions, with centers placed uniformly across the data domain. We make this naive choice so as to not allow our method to be particularly adapted to the examples below—an attempt to simulate working with data for which the underlying dynamics and distribution are truly unknown.
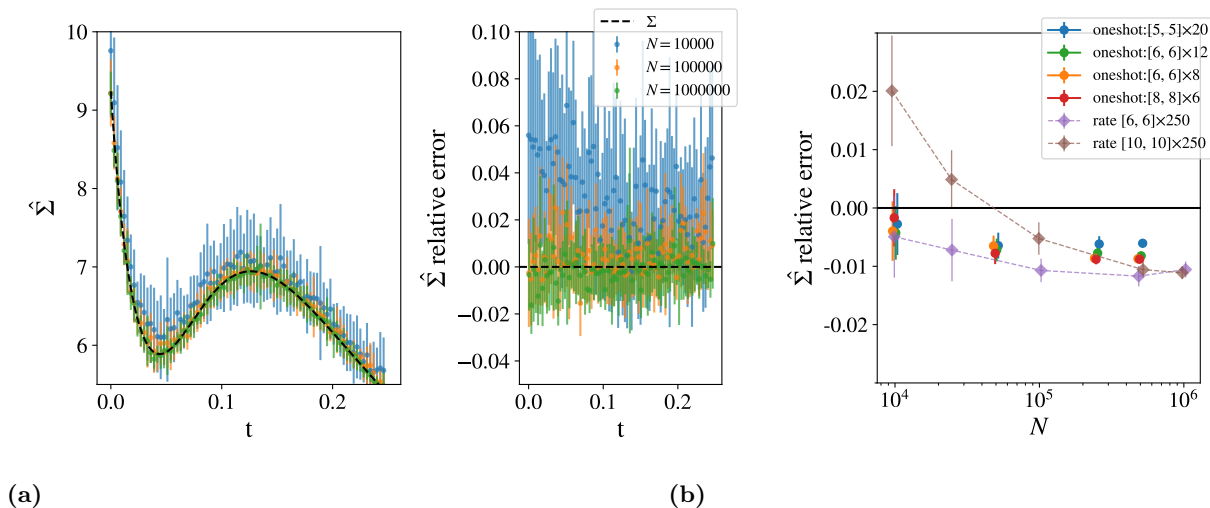
FIG. 1. (a) EP rate in free diffusion of an underdamped particle. All dynamical parameters are set to unity. The initial Gaussian distribution parameters are $(p_0, \sigma_{p_0}, \sigma_{x_0}) = (0.2, 0.3, 0.025)$. We select ≈ 80 time steps to infer the EP rate. For each time step, 10×10 Gaussian kernels in the phase space (x, p) are used. We simulated 10^4 (blue), 10^5 (orange), and 10^6 (green) trajectories with time length $\tau = 0.25$ and $\Delta t = 10^{-3}$. The black dashed line is the theoretical EP rate as a function time t. The rightmost figure shows the relative error based on 20 independent trajectory ensembles. We see that the model is mostly converged by the time it gets 10^5 data points. (b) Relative error for total EP estimation over the entire trajectory. Both one-shot (circles) and rate-based (diamonds) estimates are plotted, using various numbers of estimators in the x, p, and t directions. Note that the rate-based estimations require more data to approach errors of a few percent. The notation in the legend refers to $[n_{x_i}, n_{p_i}] \times n_{t_i}$ basis functions used. In all cases, trajectories with 250 time steps were used.

A. Rate-based estimation

If coefficients depend on time t, we find the optimal coefficients for each discretized time t_i independently. Appendix C shows this estimation is equivalent to using the short trajectories from time t_i and t_{i+1} to infer the EP during a short period of time and summing all EPs together. With this, we can divide the long-time trajectories into subtrajectories of length Δt to infer the EP. For each subtrajectory from t_i to t_{i+1}, dividing the EP with time separation Δt gives the EP rate at t_i. This is why we call it rate-based estimation. This expansion is similar to previous approaches that used short-duration currents to infer time-dependent EP rates [35].

B. One-shot estimation

Our TUR is saturable for any time-length trajectory. The previous expansion does not show this advantage of our TUR, as we measure the EP rate with short-duration currents essentially. This raises a question: Can we estimate the total EP directly instead of EP rates? This suggests using basis functions that span the whole spacetime, by letting basis functions depend on time t. Compared to estimating EP rate for each time step, this significantly reduces the number of basis functions needed to estimate the total EP as we do not use different basis functions for

each time step. That being said, the number of calculations to arrive at the final Σ is not necessarily smaller for the method at hand, because the Gaussian time kernels have infinite range. More intelligent kernels or a different optimization algorithm would likely improve the one-shot method.

V. NUMERICAL EXPERIMENTS

The first test of EP estimation concerns unconstrained diffusion. The second explores a particle constrained to move on a ring.

A. Free diffusion

Our first example is a simple but important case: vanishing external force $\boldsymbol{F} = 0$ in one dimension. The initial distribution is set to be Gaussian in both x and p. The EP rates' trend as a function of time is different based on the parameters of the initial Gaussian distribution. In Fig. 1a, we calculate EP for initial conditions that generate a nonmonotone EP rate.

First, we use rate-based estimation to infer the EP rate. At each time step, we choose 100 Gaussian kernels to cover the phase space uniformly. As seen in Fig. 1a,
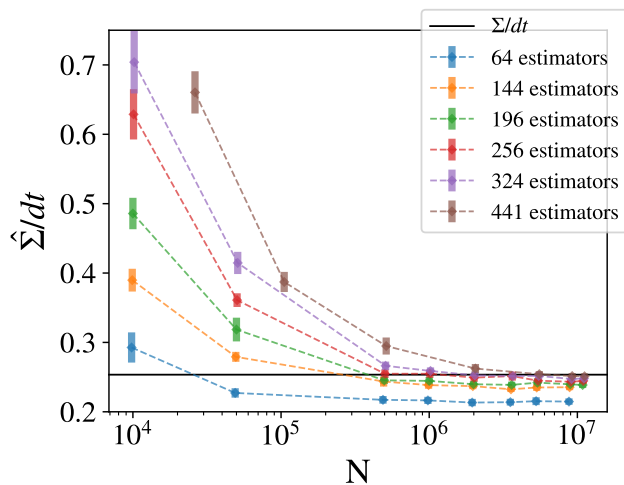
FIG. 2. Cyclic NESS EP rate estimation: We estimate the EP with different numbers of estimators and trajectories. With low number of estimators (64, 144, 196), the results converge fast with less than $\sim 10^6$ trajectories. When we increase the number of estimators, the convergent values are closer to the real EP. However, we need more trajectories for the estimated EP rate to converge.

our method produces good estimates of the EP rates at different time steps.

We can also estimate the total EP Σ over the interval using either the rate-based or the one-shot method. Figure 1b compares the methods. Notably, the one-shot method appears superior under the constraint of limited data; likely as it acts as an additional regularizer that prevents over-fitting to the variations between each successive time step. However, it does not appear to provide much advantage asymptotically.

B. Particle on a ring

Next, we explore a simulation of the NESS state of an underdamped particle on a ring under a fixed drive. We use the explicit force expression and simulated trajectories to estimate average EP directly, establishing a ground truth. In the TUR estimations, we assume no knowledge of the forcing function, only having access to trajectories.

Figure 2 illustrates the results for this cyclic underdamped particle. For each trial, we extract data for step t_i and step t_{i+1} for all trajectories. We compute the optimal weight w_{opt} for this ensemble of two successive steps—and use the EP to get the EP rate. The EP rate is estimated with different numbers of estimators for different numbers of paths from 10^4 to 10^7 . In general, too few estimators results in an asymptotic "underfitting" of the data as the model does not have sufficient flexibil-

ity to capture the true $w(x, p, t)$. More estimators yield more exact estimation after convergence, but this is also prone to overfitting until a large numbers of realizations are provided. Figure 2 shows that the standard error of the estimate decreases as the number of paths increases for any fixed number of estimators. With sufficient estimators, the estimated EP rate converges to the EP rate calculated directly.

VI. CONCLUSION

We generalized previous Langevin TURs that used Stratonovich product-based cumulant currents with weights to stochastic currents and irreversible currents. We derived modified TURs that relate statistics of these two currents to the EP. The modified TURs hold in both over- and underdamped systems and for arbitrary initial distributions, protocols, and timescales. Furthermore, the TURs can always be saturated.

We then used our TURs to study EP numerically for several underdamped Langevin examples by approximating the weight with Gaussian kernels. We studied two different methods to estimate EP—rate-based and one-shot estimation. The first only uses short-duration trajectories and the second uses entire trajectories. As a result, rate-based estimation yields the EP rate while one-shot estimation leads to a process' total EP.

This generalization opens a new window to constructing currents that probe different quantities of interest in Langevin dynamics. Additionally, our method provides a framework to estimate the EP in modified Langevin dynamics that include, for example, active Brownian motion, position-dependent damping coefficient, and the like.

Our treatment shares several aspects with the method used in Ref. [42], though here we investigated the EP from trajectories rather than distributions. We focused exclusively on underdamped examples—for which EP estimation is much more challenging. Our unregularized method to find the optimal weight is based on the algorithm in Ref. [34].

Finding a better optimization algorithm will be an important step in future applications of this TUR in higher dimensional systems. Using a stochastic method and smarter basis function choices are all potential avenues for improvement. Additionally, machine learning methods have already been used to avoid intensive computations in estimating the EP [33, 43, 44]. The successes reported here suggest that machine learning methods may assist in estimating the EP of underdamped dynamics as well.

ter for hospitality during visits and the participants of the Information Engines Workshops there. This material is based upon work supported by, or in part by, U.S. Army Research Laboratory, U.S. Army Research Office grant W911NF-21-1-0048.

Appendix A: EP in underdamped dynamics

This appendix develops several main results in underdamped Langevin dynamics. Consider a $m-$dimensional particle with initial distribution $f(\boldsymbol{x}, \boldsymbol{p}, 0)$ and governed by the Langevin equations:

$$
\begin{aligned}
d\boldsymbol{x} &= \frac{\boldsymbol{p}}{m} dt \\
d\boldsymbol{p} &= -\gamma \frac{\boldsymbol{p}}{m} dt + \boldsymbol{F}(\boldsymbol{x}, t) dt + d\boldsymbol{B}_t .
\end{aligned} \tag{A1}
$$

The corresponding time-reversed dynamics is:

$$
\begin{aligned}
d\boldsymbol{x} &= \frac{\boldsymbol{p}}{m} dt \\
d\boldsymbol{p} &= -\gamma \frac{\boldsymbol{p}}{m} dt + \boldsymbol{F}(\boldsymbol{x}, \tau - t) dt + d\boldsymbol{B}_t
\end{aligned} \tag{A2}
$$

with the initial distribution $f(\boldsymbol{x}, -\boldsymbol{p}, \tau)$, where τ is the final time of the transformation.

We first study the probability of finding the particle at $(\boldsymbol{x}+d\boldsymbol{x}, \boldsymbol{p}+d\boldsymbol{p})$ at time $t+dt$ given that the particle is at $(\boldsymbol{x}, \boldsymbol{p})$ at time t in the original dynamics. From Langevin equation, we must have $d\boldsymbol{x} = \boldsymbol{p}/m dt$. The infinitesimal Brownian motion obeys the Gaussian distribution with 0 mean and $2D dt$ variance. This gives us the conditional distribution:

$$
\begin{aligned}
&\Pr(\boldsymbol{x} + d\boldsymbol{x}, \boldsymbol{p} + d\boldsymbol{p}, t + dt | \boldsymbol{x}, \boldsymbol{p}, t) \\
&= \prod_{\alpha=1}^{m} \frac{1}{\sqrt{2\pi 2D dt}} \exp\left(-\frac{y_\alpha^2}{4D dt} \right) ,
\end{aligned} \tag{A3}
$$

where:

$$
y_\alpha = dp_\alpha + \gamma \frac{p_\alpha}{m} dt - F_\alpha(\boldsymbol{x}, t) dt \tag{A4}
$$

in each direction. For this infinitesimal trajectory Γ_{dt}: $(\boldsymbol{x}, \boldsymbol{p}, t) \to (\boldsymbol{x}+d\boldsymbol{x}, \boldsymbol{p}+d\boldsymbol{p}, t+dt)$, the conjugate time reversed trajectory $\Gamma_{dt}^\dagger$ is $(\boldsymbol{x}+d\boldsymbol{x}, -\boldsymbol{p}-d\boldsymbol{p}, t) \to (\boldsymbol{x}, -\boldsymbol{p}, t+dt)$ with time reversed dynamics. We denote the probability in the time reversed dynamics as $\Pr^\dagger(\cdot)$.

The heat in Langevin dynamics can be defined for each short trajectory:

$$
-dQ = -\gamma \frac{p}{m} \circ dx + \frac{p}{m} \circ dB_t , \tag{A5}
$$

where the first term tracks the work done by the damping and the second monitors the distribution from the random force imposed the thermal bath. The average heat is given by averaging among all trajectories. The average

EP is still defined as $\Delta S + \langle Q \rangle / T$ where ΔS is the Shannon entropy change in the system. Piecing everything together leads to:

$$
\begin{aligned}
\Sigma = \frac{dt}{\gamma T} \int d\boldsymbol{x} d\boldsymbol{p} \\
\left(-\gamma \frac{\boldsymbol{p}}{m} - \gamma T \partial_{\boldsymbol{p}} \log f(\boldsymbol{x}, \boldsymbol{p}, t) \right)^2 f(\boldsymbol{x}, \boldsymbol{p}, t) .
\end{aligned} \tag{A6}
$$

As we expect, the average EP is always nonnegative.

There is another way to define the EP for each trajectory. In underdamped Langevin dynamics, those two definitions lead to the same EP in the ensemble average. The EP assigned to each infinitesimal trajectory Γ_{dt} is:

$$
\begin{aligned}
\Sigma_{\Gamma_{dt}} &= \log \frac{\Pr(\Gamma_{dt})}{\Pr^\dagger(\Gamma_{dt}^\dagger)} \\
&= \log \frac{\Pr(\boldsymbol{x}+d\boldsymbol{x}, \boldsymbol{p}+d\boldsymbol{p}, t+dt | \boldsymbol{x}, \boldsymbol{p}, t)}{\Pr^\dagger(\boldsymbol{x}, -\boldsymbol{p}, t+dt | \boldsymbol{x}+d\boldsymbol{x}, -\boldsymbol{p}-d\boldsymbol{p}, t)} \\
&\quad \times \frac{f(\boldsymbol{x}, \boldsymbol{p}, t)}{f^\dagger(\boldsymbol{x}+d\boldsymbol{x}, -\boldsymbol{p}-d\boldsymbol{p}, t)} \\
&= \log \frac{f(\boldsymbol{x}, \boldsymbol{p}, t)}{f(\boldsymbol{x}+d\boldsymbol{x}, \boldsymbol{p}+d\boldsymbol{p}, t+dt)} + \frac{dQ}{T} ,
\end{aligned} \tag{A7}
$$

where we assume the force only depends on the position and we use middle-point discretization [45]. For a more comprehensive review on this topic, we refer readers to Refs. [45–47].

Appendix B: Average behavior of underdamped J

Definition Eq. (13) can be understood in two different ways. First, we can see by explicit averaging that it shows the proper average behavior. For the Ito part of the integral, we note that $dw \cdot dp \sim \partial_p w dp \cdot dp \sim 2D \partial_p w dt$, and write the average as:

$$
\langle J \rangle = \int dt dx dp \, w \frac{\gamma}{m} p f - \int dt dx dp \, D \partial_p w f \tag{B1}
$$

$$
= \int dt dx dp \, w \frac{\gamma}{m} p f + \int dt dx dp \, D w \frac{\partial_p f}{f} f \tag{B2}
$$

$$
= \int dt dx dp (w \, u_p^{\mathrm{irr}}) f , \tag{B3}
$$

where we assume boundary terms vanish due to the distribution function being bounded appropriately. This last term is simply an expression for $\langle w u_p^{\mathrm{irr}} \rangle$, showing the current in a way that suits our purposes, which only reflects the irreversible current part.

Another perspective comes from attempting to use the full current J^{full}; that includes contributions from u_p^{irr}

and u_p^{rev}. We decompose J^{full} into two parts:

$$
\begin{aligned}
J^{\text{full}} &\equiv \int_\Gamma w(x,p,t) \circ dp \\
&= \int_\Gamma -\gamma w(x,p,t)dx + w(x,p,t) \circ dB_t \\
&\quad + w(x,p,t)F(x,t)dt \\
&= \int_\Gamma -\gamma w(x,p,t)dx + D\partial_p w(x,p,t)dt \\
&\quad + w(x,p,t) \cdot dB_t + w(x,p,t)F(x,t)dt \\
&= J^{\text{irr}} + J^{\text{rev}} ,
\end{aligned}
\tag{B4}
$$

where:

$$
\begin{aligned}
J^{\text{irr}} = \int_\Gamma -\gamma w(x,p,t)dx &+ D\partial_p w(x,p,t)dt \\
&+ w(x,p,t) \cdot dB_t
\end{aligned}
\tag{B5}
$$

and:

$$
J^{\text{rev}} = \int_\Gamma w(x,p,t)F(x,t)dt .
\tag{B6}
$$

The average of J is equal to the average of J^{irr}, since the last term in J^{rev} vanishes upon averaging. Thus, our current J captures the irreversible part of the process and can be used to estimate the EP, since the EP only depends on J^{irr} and not J^{rev}.

Appendix C: Closed form desired weights

This section introduces the closed form of desired weight as originally derived from Ref. [34]. We start with $m-$dimensional NESS states where the weight $\boldsymbol{w}(\boldsymbol{x},\boldsymbol{p})$ does not depend on time t. The weight function $\boldsymbol{w}$ also has m components. We use k basis functions to approximate each component of the weight:

$$
w_\alpha(\boldsymbol{x},\boldsymbol{p}) = \sum_{i=1}^k c_{i\alpha}\phi_i(\boldsymbol{x},\boldsymbol{p}) ,
\tag{C1}
$$

which follows the notation from Ref. [34] and α goes from 1 to m. The variance of the stochastic current with weight $w_\alpha(\boldsymbol{x},\boldsymbol{p})$ can be written as:

$$
\frac{1}{2D}\text{var}(J_S) = \langle \int_\Gamma w_\alpha^2 dt \rangle
\tag{C2}
$$

$$
= \sum_{i,j} c_{i\alpha}c_{j\alpha}\langle \int_\Gamma \phi_i\phi_j dt \rangle
\tag{C3}
$$

$$
= \sum_{i,j} c_{i\alpha}c_{j\alpha}\Xi_{ij} ,
\tag{C4}
$$

where:

$$
\Xi_{ij} = \langle \int_\Gamma \phi_i\phi_j dt \rangle
\tag{C5}
$$

is a $k \times k$ symmetric matrix. The average of the irreversible current in $\alpha-$th direction is:

$$
\langle J^{\text{irr}}{}_\alpha \rangle = \left\langle \int_\Gamma w\gamma dx_\alpha - \frac{1}{2}\int_\Gamma dw_\alpha \cdot dp_\alpha \right\rangle
\tag{C6}
$$

$$
= \sum_i c_{i\alpha}\langle \int_\Gamma \phi_i\gamma dx - \frac{1}{2}\int_\Gamma d\phi_i \cdot dp_\alpha \rangle
\tag{C7}
$$

$$
= \sum_i c_{i\alpha}\mu_{i\alpha} ,
\tag{C8}
$$

where:

$$
\mu_{i\alpha} = \langle \int_\Gamma \phi_i\gamma dx - \frac{1}{2}\int_\Gamma d\phi_i \cdot dp_\alpha \rangle .
\tag{C9}
$$

The ratio $\mathcal{J}_\alpha$ we want to maximize with respect to $\{c_i\}_i$ is:

$$
\mathcal{J}_\alpha = \frac{\sum_{i,j} c_i c_j \mu_{i\alpha}\mu_{j\alpha}}{\sum_{i,j} c_i c_j \Xi_{ij}} .
\tag{C10}
$$

This can be done by directly asking the partial derivatives to vanish which leads to the maximum of $\mathcal{J}_\alpha$:

$$
\mathcal{J}_{\alpha\max} = \sum_{i,j} \mu_{i\alpha}\Xi_{ij}^{-1}\mu_{j\alpha} .
\tag{C11}
$$

We achieve the maximum when $c_{i\alpha} \sim \sum_j \Xi_{ij}^{-1}\mu_{j\alpha}$, where Ξ^{-1} is the inverse of Ξ. The $\sim$ sign comes from $\mathcal{J}$ being invariant under rescaling c. For multidimensional system, we need to compute the Ξ matrix once and μ for each direction.

For nonNESS states, we first choose that our coefficients $c_{i\alpha}$ depend on time t which we denote as $c_{i\alpha}(t_n)$ at time step t_n:

$$
w_\alpha(\boldsymbol{x},\boldsymbol{p},t) = \sum_i^k c_{i\alpha}(t)\phi_i(\boldsymbol{x},\boldsymbol{p}) .
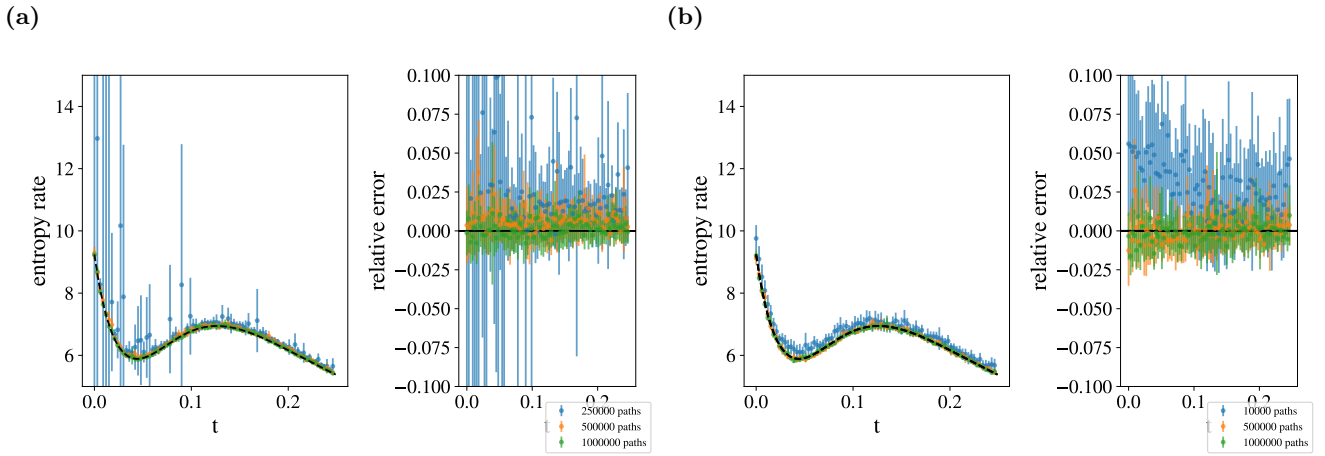\tag{C12}
$$

The variance of current J_S can be written as:

$$
\text{var}(J_{S\alpha}) = \left\langle \int_{t_0}^{t_1} w_\alpha^2 dt \right\rangle + \cdots + \left\langle \int_{t_{N-1}}^{t_N} w_\alpha^2 dt \right\rangle .
\tag{C13}
$$

Discretizing this by taking the value of the starting point of each integral:

$$
\begin{aligned}
\text{var}(J_{S\alpha})_{\text{start}} = c_{i\alpha}(t_0)c_{j\alpha}(t_0)\left\langle \int_{t_0}^{t_1} \phi_i\phi_j dt \right\rangle + \cdots \\
+ c_{i\alpha}(t_{N-1})c_{j\alpha}(t_{N-1})\left\langle \int_{t_{N-1}}^{t_N} \phi_i\phi_j dt \right\rangle .
\end{aligned}
\tag{C14}
$$

Using ending point discretization leads us to:

$$
\begin{aligned}
\text{var}(J_{S\alpha})_{\text{end}} = c_{i\alpha}(t_1)c_{j\alpha}(t_1)\left\langle \int_{t_0}^{t_1} \phi_i\phi_j dt \right\rangle + \cdots \\
+ c_{i\alpha}(t_N)c_{j\alpha}(t_N)\left\langle \int_{t_{N-1}}^{t_N} \phi_i\phi_j dt \right\rangle .
\end{aligned}
\tag{C15}
$$

(a)   **(b)**

FIG. 3. Results for the (a) unregularized and (b) regularized estimation. The blue data represents the behavior when given 250,000 (10,000) data points for the unregularized(regularized) models. Orange and green data are 500,000 and 1,000,000 data points, respectively, in both panels. Note that without the L2 norm regularization, the results are very messy even for 250,000 data points while the regularized data is already well behaved, if biased, for only 10,000 data points (compare blue to blue). The converged behavior is quite similar (compare green to green), but the regularized model reaches convergence must faster.

These two are equal to each other as $dt \to 0$ since we integrate with time dt. To make the expression more symmetric, we average these two:

$$\text{var}(J_{S\alpha}) = \frac{1}{2}\text{var}(J_{S\alpha})_{\text{start}} + \frac{1}{2}\text{var}(J_{S\alpha})_{\text{end}} \ . \quad \text{(C16)}$$

It can be written as:

$$\text{var}(J_S) = \frac{1}{2}\sum_i c_{i\alpha}(t_0)c_{j\alpha}(t_0)\Xi(t_0)_{ij}$$
$$+ \sum_{n=1}^{N-1}\sum_i c_{i\alpha}(t_n)c_{j\alpha}(t_n)\Xi(t_n)_{ij}$$
$$+ \frac{1}{2}\sum_i c_{i\alpha}(t_N)c_{j\alpha}(t_N)\Xi(t_N)_{ij} \ , \quad \text{(C17)}$$

where:

$$\Xi_{ij}(t_n) = \left\langle \int_{t_n}^{t_{n+1}} \phi_i\phi_j dt \right\rangle$$
$$= \langle \phi_i\phi_j\Delta t\rangle \quad \text{(C18)}$$

is a symmetric matrix as a function of time step.

The average of J^{irr} can be written as:

$$\langle J^{\text{irr}}{}_\alpha\rangle = \left\langle \int_{t_0}^{t_1} w\gamma dx_\alpha \right\rangle + \cdots + \left\langle \int_{t_{N-1}}^{t_N} w\gamma dx_\alpha \right\rangle$$
$$- \frac{1}{2}\left\langle \int_{t_0}^{t_1} dw_\alpha \cdot dp_\alpha \right\rangle - \cdots - \frac{1}{2}\left\langle \int_{t_{N-1}}^{t_N} dw_\alpha \cdot dp_\alpha \right\rangle$$
$$= \sum_{n=0}^{N}\sum_i c_{i\alpha}(t_n)\mu_{i\alpha}(t_n) \ , \quad \text{(C19)}$$

where:

$$\mu_{i\alpha}(t_n) = \langle\phi_i(x_\alpha(t_n), p_\alpha(t_n))\gamma dx_\alpha$$
$$- \frac{1}{2}\phi_i(x_\alpha(t_n), p_\alpha(t_n))(p_\alpha(t_{n+1}) - p_\alpha(t_{n-1}))\rangle$$
$$\text{for } n \neq 0, N \quad \text{(C20)}$$
$$= \langle\phi_i(x_\alpha(t_0), p_\alpha(t_0))\gamma dx_\alpha$$
$$+ \frac{1}{2}\phi_i(x_\alpha(t_0), p_\alpha(t_0))(p_\alpha(t_1) - p_\alpha(t_0))\rangle$$
$$\text{for } n = 0 \quad \text{(C21)}$$
$$= -\langle\frac{1}{2}\phi_i(x_\alpha(t_N), p_\alpha(t_N))(p_\alpha(t_N) - P_\alpha(t_{N-1}))\rangle$$
$$\text{for } n = N. \quad \text{(C22)}$$

Following the same algebra in the NESS state, the maximum of ratio $\mathcal{J}_\alpha$ is:

$$\mathcal{J}_{\alpha\text{max}} = \sum_{n=1}^{N}\sum_{i,j}\mu_{i\alpha}(t_n)\left(\Xi(t_n)^{-1}\right)_{ij}\mu_{j\alpha}(t_n) \ . \quad \text{(C23)}$$

This result Eq. (C23) clearly shows that even if we feed the long time trajectories into this estimation scheme, the total EP estimated is equal to sum of EPs in each short duration Δt. This is why we call it rate-based estimation when coefficients have time dependence. It is equivalent to estimating the entropy rate at each time step.

If our basis functions have time dependence:

$$w_\alpha(\boldsymbol{x}, \boldsymbol{p}) = \sum_i^N c_{i\alpha}\phi_i(\boldsymbol{x}, \boldsymbol{p}, t) \ , \quad \text{(C24)}$$

the maximum ratio is similar to NESS state case. The variance of the stochastic current is:

$$\frac{1}{2D}\text{var}(J_S) = \left\langle \int_\Gamma w_\alpha^2 dt \right\rangle \tag{C25}$$

$$= \sum_{i,j} c_{i\alpha} c_{j\alpha} \left\langle \int_\Gamma \phi_i(t)\phi_j(t)dt \right\rangle \tag{C26}$$

$$= \sum_{i,j} c_{i\alpha} c_{j\alpha} \Xi_{ij} , \tag{C27}$$

where:

$$\Xi_{ij} = \left\langle \int_\Gamma \phi_i(t)\phi_j(t)dt \right\rangle . \tag{C28}$$

And the discretized version is:

$$\Xi_{ij} = \left\langle \sum_{n=0}^{N-1} \phi_i(\boldsymbol{x}(t_n),\boldsymbol{p}(t_n),t_n)\phi_j(\boldsymbol{x}(t_n),\boldsymbol{p}(t_n),t_n)\Delta t \right\rangle \tag{C29}$$

in starting point discretization or:

$$\Xi_{ij} = \left\langle \sum_{n=1}^{N} \phi_i(\boldsymbol{x}(t_n),\boldsymbol{p}(t_n),t_n)\phi_j(\boldsymbol{x}(t_n),\boldsymbol{p}(t_n),t_n)\Delta t \right\rangle \tag{C30}$$

in ending point discretization.

The average of the irreversible current in $\alpha-$th direction is:

$$\langle J^{\text{irr}}{}_\alpha \rangle = \left\langle \int_\Gamma w\gamma dx_\alpha - \frac{1}{2}\int_\Gamma dw_\alpha \cdot dp_\alpha \right\rangle \tag{C31}$$

$$= \sum_i c_{i\alpha} \left\langle \int_\Gamma \phi_i \gamma dx - \frac{1}{2}\int_\Gamma d\phi_i \cdot dp_\alpha \right\rangle \tag{C32}$$

$$= \sum_i c_{i\alpha} \mu_{i\alpha} , \tag{C33}$$

where:

$$\mu_{i\alpha} = \left\langle \int_\Gamma \phi_i \gamma dx - \frac{1}{2}\int_\Gamma d\phi_i \cdot dp_\alpha \right\rangle . \tag{C34}$$

The discretized version is:

$$\mu_{i\alpha} = \left\langle \sum_{n=0}^{N-1} \phi_i(\boldsymbol{x}(t_n),\boldsymbol{p}(t_n),t_n)\gamma(x_\alpha(t_{n+1})-x_\alpha(t_n)) - \right.$$
$$\frac{1}{2}(\phi_i(\boldsymbol{x}(t_{n+1}),\boldsymbol{p}(t_{n+1}),t_{n+1})-\phi_i(\boldsymbol{x}(t_n),\boldsymbol{p}(t_n),t_n))$$
$$\left. \times (p_\alpha(t_{n+1})-p_\alpha(t_n)) \right\rangle . \tag{C35}$$

The maximum of $\mathcal{J}_\alpha$ is then:

$$\mathcal{J}_{\alpha\max} = \sum_{i,j} \mu_{i\alpha} \Xi_{ij}^{-1} \mu_{j\alpha} . \tag{C36}$$

Those above are all for EP in one direction. To account the total EP, we need to sum over all directions:

$$\Sigma = \sum_\alpha \mathcal{J}_{\alpha\max} . \tag{C37}$$

For all scenarios mentioned above, we encounter the problem finding the maximum of a ratio with the form of:

$$\mathcal{J} = \frac{\sum_{i,j} c_i c_j \mu_i \mu_j}{\sum_{i,j} c_i c_j \Xi_{ij}} \tag{C38}$$

with respect to c_i. Since this ratio is invariant under rescaling c_i: $c_i \to \kappa c_i$, we can set $\sum_i c_i \mu_i = 1$. The challenge turns out to be finding the minimum of $\sum_{i,j} c_i c_j \Xi_{ij}$ given the constraint $\sum_i c_i \mu_i = 1$. To avoid overfitting when the number of estimators—or the dimension of c_i—is large compared to the size of the data set, we include regularization. The Lagrangian function now is:

$$\mathcal{L} = \sum_{i,j} c_i c_j \Xi_{ij} + \beta \sum_i c_i^2 + \lambda(\sum_i c_i \mu_i - 1) \tag{C39}$$

$$= \sum_{i,j} c_i c_j (\Xi_{ij} + \beta\delta_{ij}) + \lambda(\sum_i c_i \mu_i - 1) . \tag{C40}$$

With L-2 regularization, the new result is:

$$\sum_{i,j} \mu_i \Xi_{ij}^{-1} \mu_j \to \sum_{i,j} \mu_i (\Xi + \beta I)_{ij}^{-1} \mu_j . \tag{C41}$$

We can expand this result in powers of β:

$$\sum_{i,j} \mu_i (\Xi + \beta I)_{ij}^{-1} \mu_j \sim \sum_{i,j} \mu_i \Xi_{ij}^{-1} \mu_j - \beta \sum_{i,j} \mu_i \Xi_{ij}^{-2} \mu_j$$
$$+ \beta^2 \sum_{i,j} \mu_i \Xi_{ij}^{-3} \mu_j + \mathcal{O}(\beta^3) . \tag{C42}$$

Assuming β is small, the regularization decrease the unregularized result. This bias was minor for all cases tested—changing the relative error by no more than half a percent. See Figs. 3b and 5 which compare unregularized and regularized data sets. For all cases, we set $\beta = N^{-2}$.

Appendix D: Model details

1. Free diffusion

This appendix presents the main results for free diffusion EP in the underdamped regime. The Langevin equations are:

$$dx = p/m \ dt , \tag{D1}$$
$$dp = -\gamma p/m \ dt + dB_t . \tag{D2}$$

And, the probability distribution $f(x,p,t)$ evolution obeys the Krammer's equation:

$$\partial_t f + \partial_x(p/mf) + \partial_p(-\gamma p/m - \gamma T\partial_p f/f) = 0 . \tag{D3}$$

The Green function of Eq. (D3) is:

$$f(x, p, x', p', t) = \frac{1}{2\pi\sigma_X\sigma_P\sqrt{1-\beta^2}}\exp\left(-\frac{1}{2(1-\beta^2)}\right.$$
$$\left[\frac{(x-\mu_X)^2}{\sigma_X^2} + \frac{(p-\mu_P)^2}{\sigma_P^2}\right.$$
$$\left.\left. - \frac{2\beta(x-\mu_X)(p-\mu_P)}{\sigma_X\sigma_P}\right]\right), \tag{D4}$$

where:

$$\sigma_X^2 = \frac{mT}{\gamma^2}\left[1 + 2\frac{\gamma}{m}t - \left(2 - e^{-\frac{\gamma}{m}t}\right)^2\right] \tag{D5}$$

$$\sigma_P^2 = mT\left(1 - e^{-2\frac{\gamma}{m}t}\right) \tag{D6}$$

$$\beta = \frac{mT}{\gamma\sigma_X\sigma_P}\left(1 - e^{-\frac{\gamma}{m}t}\right)^2 \tag{D7}$$

$$\mu_X = x' + \frac{1}{\gamma}\left(1 - e^{-\frac{\gamma}{m}t}\right)p' \text{, and} \tag{D8}$$

$$\mu_P = p'e^{-\frac{\gamma}{m}t} . \tag{D9}$$

If the initial probability distribution is a Gaussian distribution that is uncorrelated in position and momentum, i.e.,

$$f(x, p, 0) = \frac{1}{2\pi\sigma_{x_0}\sigma_{p_0}}e^{-\frac{(x-x_0)^2}{2\sigma_{x_0}^2} - \frac{(p-p_0)^2}{2\sigma_{p_0}^2}} , \tag{D10}$$

then the distribution is always Gaussian with mean $\boldsymbol{\mu}$ and variance $\boldsymbol{\Sigma}$, where:

$$\boldsymbol{\mu}(t) = (\mu_x, \mu_p)^\top \tag{D11}$$

$$\boldsymbol{\Sigma}(t) = \begin{pmatrix} \sigma_x^2 & \text{cov}(x, p) \\ \text{cov}(x, p) & \sigma_p^2 \end{pmatrix} \tag{D12}$$

with:

$$\mu_x = x_0 + \frac{1}{\gamma}(1 - e^{-\frac{\gamma}{m}t})p_0 \tag{D13}$$

$$\mu_p = p_0 e^{-\frac{\gamma}{m}t} \tag{D14}$$

and:

$$\text{cov}(x, p) = \frac{1}{\gamma}(1 - e^{-\frac{\gamma}{m}t})(mT - mTe^{-\frac{\gamma}{m}t} + \sigma_{p_0}^2 e^{-\frac{\gamma}{m}t}) \tag{D15}$$

$$\sigma_p^2 = (\sigma_{p_0}^2 - mT)e^{-2\frac{\gamma}{m}t} + mT \tag{D16}$$

$$\sigma_x^2 = -\frac{1}{\gamma^2}\left(1 - e^{-\frac{\gamma}{m}t}\right)$$
$$\times \left(mT(3 - e^{-\frac{\gamma}{m}t}) - \sigma_{p_0}^2(1 - e^{-\frac{\gamma}{m}t})\right)$$
$$+ \frac{2T}{\gamma}t + \sigma_{x_0}^2 . \tag{D17}$$

To compute the EP, the heat Q transferred to the bath is equal to the negative change in kinetic energy:

$$Q = -\frac{1}{2m}(\mu_p^2 + \sigma_p^2 - p_0^2 - \sigma_{p_0}^2) . \tag{D18}$$

The EP rate is given by:

$$\Sigma = \partial_t\left(Q/T + \frac{1}{2}\log\det\boldsymbol{\Sigma}(t) - \frac{1}{2}\log\det\boldsymbol{\Sigma}(0)\right)$$
$$= \partial_t\left(-\mu_p^2 - \sigma_p^2 + \frac{1}{2}\log\det\boldsymbol{\Sigma}\right) . \tag{D19}$$

The u_p^{irr} in this case is:

$$u_p^{\text{irr}} = -\gamma\frac{p}{m} - \gamma T\partial_p \log f(x, p, t)$$
$$= \left(-\frac{\gamma}{m} - \frac{\gamma T}{(-1+\beta^2)\sigma_p^2}\right)p$$
$$+ \frac{\gamma T\beta}{(-1+\beta^2)\sigma_x\sigma_p}x + \frac{\gamma T\mu_p}{(-1+\beta^2)\sigma_p^2}$$
$$- \frac{\gamma T\beta\mu_x}{(-1+\beta^2)\sigma_x\sigma_p} . \tag{D20}$$

2. Particle on a ring

In this model, we study a particle on a ring of circumference 3 driven by a constant force of $F = 1$ (in units of k_BT per distance). The potential energy around the ring is composed of three sinusoidal wells. Two of these wells are shallow on one side, and one of them is deep on both sides. With sufficiently long time, the system reaches a NESS state. Figures 4a and 4b show the potential and NESS probability distribution in (x, p) phase space. The depths of the shallow and deep barriers are $1.5k_BT$ and $2.25k_BT$, respectively.

Appendix E: Estimator details

This appendix discusses how to determine parameters in Gaussian kernels. We first consider kernels for the rate-base estimation at time t. For an m-dimensional system, the phase space dimension is $2m$. We need to approximate an m-dimensional weight $\boldsymbol{w}(\boldsymbol{x}, \boldsymbol{p}, t)$. We denote its α component as $w_\alpha(\boldsymbol{x}, \boldsymbol{p}, t)$. For each component, we use the same k Gaussian kernels to approximate it; denoted as $G_i(\boldsymbol{x}, \boldsymbol{p})$. The Gaussian kernels have the form:

$$G_i(\boldsymbol{x}, \boldsymbol{p}) = e^{-(\boldsymbol{x}-\bar{\boldsymbol{x}}_i)^\top\Sigma_x^{-1}(\boldsymbol{x}-\bar{\boldsymbol{x}}_i) - (\boldsymbol{p}-\bar{\boldsymbol{p}}_i)^\top\Sigma_p^{-1}(\boldsymbol{p}-\bar{\boldsymbol{p}}_i)} , \tag{E1}$$

where $(\bar{\boldsymbol{x}}_i^\top, \bar{\boldsymbol{p}}_i^\top)$ are the i-th kernel's center in the phase space. Σ_x and Σ_p are the bandwidth of Gaussian kernels—two diagonal positive diagonal matrices. We choose centers to be on a rectangular grid. Along each grid direction, we set n points and $k = n^{2m}$.

We first determine the maximum and minimum in phase space of all trajectories as $\boldsymbol{x}_{\min}$, $\boldsymbol{x}_{\max}$, $\boldsymbol{p}_{\min}$, and $\boldsymbol{p}_{\max}$. For each direction q in phase space $(q = x_\alpha, p_\alpha)$, the bandwidth is determined by $\Sigma_q = (q_{\max} - q_{\min} + $

(a)
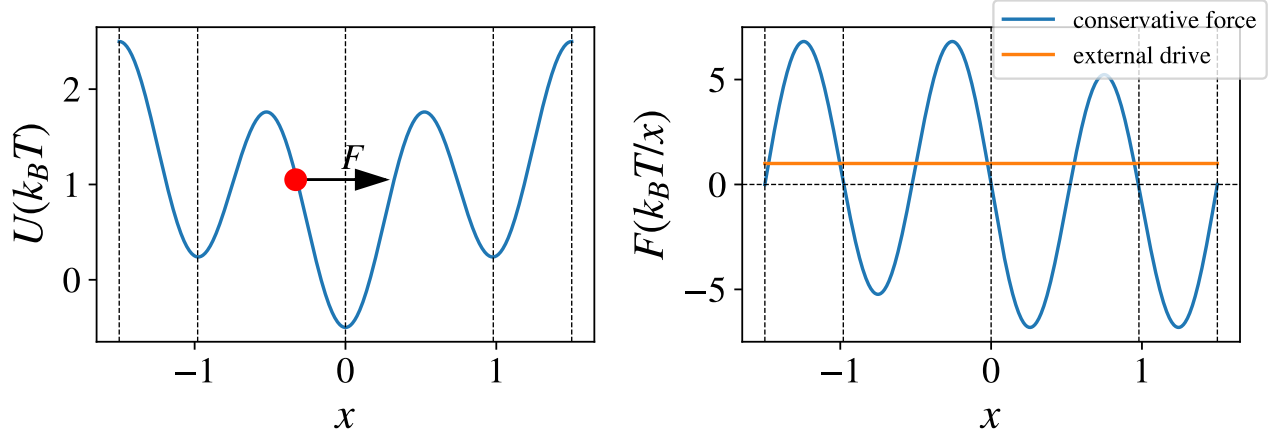
(b)
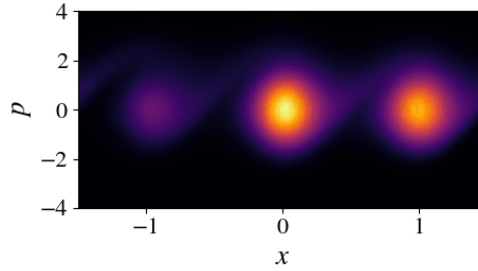
FIG. 4. (a) Sketch of the NESS model: An underdamped particle trapped in a ring of length 3 driven by a constant force F within a cyclic potential: $V(x+3) = V(x)$. (b) NESS probability distribution of the particle.

$\sigma_q)/(n-2)$, where σ_q is the standard deviation of trajectories data of q at time t. And, the centers in the q direction are $\bar{q}_\alpha = \{q_{\min} - \sigma_q + (j - \frac{1}{2}) \cdot \sigma_q\}_{j=0}^n$. The centers lie on a $2m$-dimension grid of each direction's centers.

For one-shot estimation, we add time dependence to the Gaussian kernels:

$$G_i(\boldsymbol{x}, \boldsymbol{p}, t) = e^{-\frac{1}{2}(\boldsymbol{x} - \bar{\boldsymbol{x}}_i)^\top \Sigma_x^{-1}(\boldsymbol{x} - \bar{\boldsymbol{x}}_i) - \frac{1}{2}(\boldsymbol{p} - \bar{\boldsymbol{p}}_i)^\top \Sigma_p^{-1}(\boldsymbol{p} - \bar{\boldsymbol{p}}_i)}$$
$$\cdot e^{-(t-t_i)^2/2\sigma_t^2} . \tag{E2}$$

In the time direction, the number of estimators is chosen to be n_t. We let our estimators cover a wider range than $[0, \tau]$. The bandwidth and centers are set to be $\sigma_t = \tau/(n_t - 2)$ and $\{-\frac{1}{2}\sigma_t + (i-1)\sigma_t\}_{i=1}^{n_t}$, respectively.

The number n of estimators in each direction can be tuned in each direction. If n is too small, the Gaussian kernels cannot capture the behavior of the real weights and the estimates converge to a quantity less than the actual EP. Large n, however, leads to overfitting and this requires more trajectories to converge. For each different case, we used different numbers of estimators. Figure 5 shows how different numbers of estimators converge for different numbers of paths for the particle on a ring NESS system. This plot is using an un-regularized method, to

provide comparison with Fig 2 in the main text. We see that the general trend is the same as Fig 2, but convergence is messier and slower. A general trend is that this estimation scheme underestimates the EP (rate) when the number of estimators is too small. With a finite number of trajectories, however, a large high number of estimators encounters overfitting. For a fixed number of estimators, we see that the standard error decreases as number of trajectories increases. With more estimators, the average estimation is closer to the real value of EP rate.

Appendix F: Simulation Detail

The free diffusion simulation used the Euler-Maryama integration method to sample trajectories. The cyclic NESS simulations additionally used 4th-order Runge-Kutta for the deterministic portion of the integration. For the cyclic NESS system, the steady state was approximated by running the simulation until stationarity was reached. For all simulations, Python's NumPy random generator was used to produce realizations of dB_t. In all
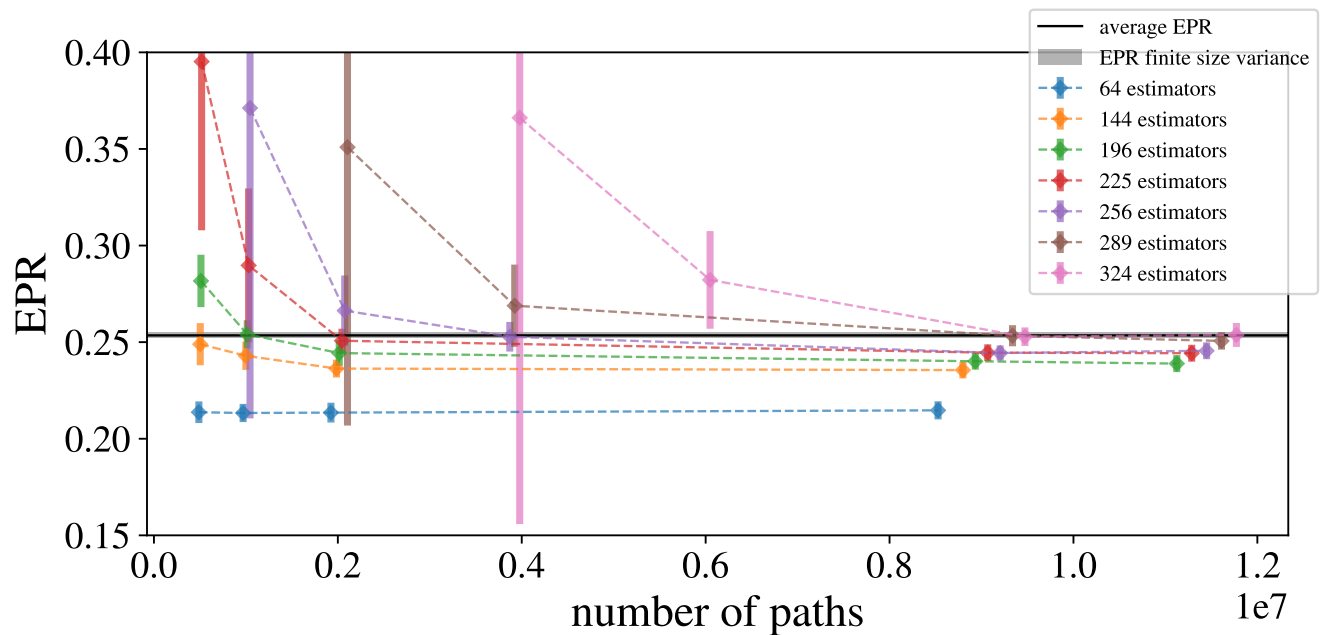
FIG. 5. Unregularized entropy production rate (EPR) estimation for the cyclic NESS. Here, we must go to 10^7 trajectories to converge to the correct value when the data is not regularized. The key parts of the algorithm scale with (num estimators)^2(num paths) and (num estimators)^6. The first term tends to dominate because so much data is needed and the computation becomes computationally quite expensive.

estimation problems, $dt = 10^{-3}$, with $\gamma = k = m = T = 1$. For the NESS system, to assure faithful dynamics, trajectories were simulated using $dt = 2 \times 10^{-4}$—but only every 5th step was kept to simulate trajectories measured with a time interval of 10^{-3}.

[1] A. C. Barato and U. Seifert, Thermodynamic uncertainty relation for biomolecular processes, Phys. Rev. Lett. **114**, 158101 (2015).

[2] T. R. Gingrich, J. M. Horowitz, N. Perunov, and J. L. England, Dissipation bounds all steady-state current fluctuations, Phys. Rev. Lett. **116**, 120601 (2016).

[3] J. M. Horowitz and T. R. Gingrich, Proof of the finite-time thermodynamic uncertainty relation for steady-state currents, Phys. Rev. E **96**, 020103 (2017).

[4] J. M. Horowitz and T. R. Gingrich, Thermodynamic uncertainty relations constrain non-equilibrium fluctuations, Nat. Phys **16**, 15 (2020).

[5] K. Liu, Z. Gong, and M. Ueda, Thermodynamic uncertainty relation for arbitrary initial states, Phys. Rev. Lett. **125**, 140602 (2020).

[6] T. Koyuk and U. Seifert, Thermodynamic uncertainty relation for time-dependent driving, Phys. Rev. Lett. **125**, 260604 (2020).

[7] J. S. Lee, J.-M. Park, and H. Park, Universal form of thermodynamic uncertainty relation for langevin dynamics, Phys. Rev. E **104**, L052102 (2021).

[8] Z. Cao, J. Su, H. Jiang, and Z. Hou, Effective entropy production and thermodynamic uncertainty relation of active Brownian particles, Phys. Fluids **34** (2022).

[9] P. P. Potts and P. Samuelsson, Thermodynamic uncertainty relations including measurement and feedback, Phys. Rev. E **100**, 052137 (2019).

[10] P. Pietzonka, A. C. Barato, and U. Seifert, Universal bounds on current fluctuations, Phys. Rev. E **93**, 052145 (2016).

[11] M. PoLett.ini, A. Lazarescu, and M. Esposito, Tightening the uncertainty principle for stochastic currents, Phys. Rev. E **94**, 052104 (2016).

[12] K. Proesmans and C. Van den Broeck, Discrete-time thermodynamic uncertainty relation, EPL **119**, 20001 (2017).

[13] A. Dechant and S.-i. Sasa, Current fluctuations and transport efficiency for general langevin systems, J. Stat. Mech.: Theory Exp. **2018** (6), 063209.

[14] A. C. Barato, R. Chetrite, A. Faggionato, and D. Gabrielli, Bounds on current fluctuations in periodically driven systems, New J. Phys. **20**, 103023 (2018).

[15] K. Macieszczak, K. Brandner, and J. P. Garrahan, Unified thermodynamic uncertainty relations in linear response, Phys. Rev. Lett. **121**, 130601 (2018).

[16] K. Brandner, T. Hanazato, and K. Saito, Thermodynamic bounds on precision in ballistic multiterminal transport, Phys. Rev. Lett. **120**, 090601 (2018).

[17] T. Koyuk and U. Seifert, Operationally accessible bounds on fluctuations and entropy production in periodically driven systems, Phys. Rev. Lett. **122**, 230601 (2019).

[18] H.-M. Chun, L. P. Fischer, and U. Seifert, Effect of a magnetic field on the thermodynamic uncertainty relation, Phys. Rev. E **99**, 042128 (2019).

[19] T. Van Vu and Y. Hasegawa, Uncertainty relations for time-delayed langevin systems, Phys. Rev. E **100**, 012134 (2019).

[20] A. Dechant, Multidimensional thermodynamic uncertainty relations, J. Phys. A **52**, 035001 (2018).

[21] Y. Hasegawa and T. Van Vu, Fluctuation theorem uncertainty relation, Phys. Rev. Lett. **123**, 110602 (2019).

[22] G. Guarnieri, G. T. Landi, S. R. Clark, and J. Goold, Thermodynamics of precision in quantum nonequilibrium steady states, Phys. Rev. Res. **1**, 033021 (2019).

[23] K. Proesmans and J. M. Horowitz, Hysteretic thermodynamic uncertainty relation for systems with broken time-reversal symmetry, J. Stat. Mech.: Theory Exp. **2019** (5), 054005.

[24] T. Van Vu and Y. Hasegawa, Uncertainty relation under information measurement and feedback control, J. Phys. A **53**, 075001 (2020).

[25] A. M. Timpanaro, G. Guarnieri, J. Goold, and G. T. Landi, Thermodynamic uncertainty relations from exchange fluctuation theorems, Phys. Rev. Lett. **123**, 090604 (2019).

[26] Y. Hasegawa, Quantum thermodynamic uncertainty relation for continuous measurement, Phys. Rev. Lett. **125**, 050601 (2020).

[27] K. J. Ray, A. B. Boyd, G. Guarnieri, and J. P. Crutchfield, Thermodynamic uncertainty theorem, Phys. Rev. E **108**, 054126 (2023).

[28] Y. Hasegawa and T. Van Vu, Uncertainty relations in stochastic processes: An information inequality approach, Phys. Rev. E **99**, 062126 (2019).

[29] A. Dechant and S.-i. Sasa, Fluctuation–response inequality out of equilibrium, Proc. Natl. Acad. Sci. U.S.A **117**, 6430 (2020).

[30] C. Dieball and A. Godec, Direct route to thermodynamic uncertainty relations and their saturation, Phys. Rev. Lett. **130**, 087101 (2023).

[31] J. Li, J. M. Horowitz, T. R. Gingrich, and N. Fakhri, Quantifying dissipation using fluctuating currents, Nat. Commun **10**, 1666 (2019).

[32] S. K. Manikandan, D. Gupta, and S. Krishnamurthy, Inferring entropy production from short experiments, Phys. Rev. Lett. **124**, 120603 (2020).

[33] S. Otsubo, S. Ito, A. Dechant, and T. Sagawa, Estimating entropy production by machine learning of short-time fluctuating currents, Phys. Rev. E **101**, 062106 (2020).

[34] T. Van Vu, Y. Hasegawa, *et al.*, Entropy production estimation with optimal current, Phys. Rev. E **101**, 042138 (2020).

[35] S. Otsubo, S. K. Manikandan, T. Sagawa, and S. Krishnamurthy, Estimating time-dependent entropy production from non-equilibrium trajectories, Commun. Phys. **5**, 11 (2022).

[36] T. Van Vu and Y. Hasegawa, Uncertainty relations for underdamped Langevin dynamics, Phys. Rev. E **100**, 032130 (2019).

[37] L. P. Fischer, H.-M. Chun, and U. Seifert, Free diffusion bounds the precision of currents in underdamped dynamics, Phys. Rev. E **102**, 012120 (2020).

[38] I. Di Terlizzi and M. Baiesi, A thermodynamic uncertainty relation for a system with memory, J. Phys. A **53**, 474002 (2020).

[39] T. Van Vu and Y. Hasegawa, Thermodynamic uncertainty relations under arbitrary control protocols, Phys. Rev. Res. **2**, 013060 (2020).

[40] U. Seifert, Stochastic thermodynamics, fluctuation theorems and molecular machines, Rep. Prog. Phys. **75**, 126001 (2012).

[41] A. Dechant and Y. Sakurai, Thermodynamic interpretation of Wasserstein distance, arXiv preprint arXiv:1912.08405 (2019).

[42] S. Lee, D.-K. Kim, J.-M. Park, W. K. Kim, H. Park, and J. S. Lee, Multidimensional entropic bound: Estimator of entropy production for langevin dynamics with an arbitrary time-dependent protocol, Phys. Rev. Res. **5**, 013194 (2023).

[43] D.-K. Kim, Y. Bae, S. Lee, and H. Jeong, Learning entropy production via neural networks, Phys. Rev. Lett.

125, 140604 (2020).

[44] E. Kwon and Y. Baek, α-divergence improves the entropy production estimation via machine learning, Phys. Rev. E **109**, 014143 (2024).

[45] R. E. Spinney and I. J. Ford, Entropy production in full phase space for continuous stochastic dynamics, Phys. Rev. E **85**, 051113 (2012).

[46] K. Sekimoto, Stochastic energetics (2010).

[47] L. Peliti and S. Pigolotti, *Stochastic thermodynamics: an introduction* (Princeton University Press, 2021).